Applied Catalysis B: Environmental 152–153 (2014) 88–98

Contents lists available at ScienceDirect

Applied Catalysis B: Environmental

journal homepage: www.elsevier.com/locate/apcatb

Influence of the surface potassium species in Fe–K/Al_2O_3 catalysts on the soot oxidation activity in the presence of NO_x

M.E. Gálvez[a,*,1], S. Ascaso[a], P. Stelmachowski[b], P. Legutko[b], A. Kotarba[b], R. Moliner[a], M.J. Lázaro[a]

[a] Instituto de Carboquímica, CSIC, Miguel Luesma Castán, 4, 50018 Zaragoza, Spain
[b] Jagiellonian Univeristy, Ingardena, 3, 30060 Krakow, Poland

ARTICLE INFO

Article history:
Received 22 November 2013
Received in revised form 14 January 2014
Accepted 20 January 2014
Available online 27 January 2014

Keywords:
Alkali promoter
Soot oxidation
NO_x reduction
Exhaust-gas cleaning
Supported catalysts

ABSTRACT

Cordierite monolith-supported and powder Fe–K/Al_2O_3 catalysts were prepared and thoroughly characterized by bulk (XRD, Raman spectroscopy, XRF, ICP–OES, TPR) and surface (XPS, IR, N_2-BET, NO_x-TPD, K-TPD) sensitive methods. The catalytic activity was tested in TPO (temperature programmed oxidation) of model soot. The influence of the calcination temperature, i.e. 450 and 650 °C, on the catalysts physicochemical properties and reactivity, type of surface states of K promoter and their role in the soot oxidation mechanism in the presence of NO_x was evaluated. In the catalysts calcined at 450 °C potassium was found to be mostly as free KNO_3 whereas calcination at 650 °C successfully transformed KNO_3 into K_2O, which during the soot oxidation yielded K_2CO_3 species. Such carbonates underwent decomposition in the presence of the oxygen surface groups of the support, leading to the formation of active basic O^{2-} groups. NO_x species were found to adsorb strongly on these O^{2-} sites. The increased stability of thus formed NO_x-species resulted in lower soot oxidation activity. In the same time, the catalysts calcined at 650 °C evidenced higher ability towards the reduction of NO_x, occurring simultaneously with the soot oxidation process. Additionally, the higher calcination temperature led to significantly higher stability of K promoter species as evidenced by potassium thermodesorption experiments. An overall schematic model of the catalyst morphology and relative distribution of the active components (K, Fe) over the Al_2O_3 support is proposed.

1. Introduction

As a result of the particular features of fuel combustion under lean conditions, soot and NO_x emission control in diesel exhausts represents a real challenge nowadays. Evidences of the serious hazard to human health and to the environment that these pollutants pose, have resulted in the introduction of more and more stringent legislation concerning their emission limits [1].

Still, due to their enhanced fuel economy and durability, diesel engines represent an important part of the light-duty vehicle market. Therefore, considerable efforts have been made in the last decades to reduce their negative environmental impact. The well-known trade-off between soot and NO_x formation sets a limit to emission control via engine modifications, thus, after-treatment technologies had to be considered. NO_x emission can be controlled by means of Selective Catalytic Reduction (SCR) and NO_x Storage-Reduction (NSR) [2,3]. Soot can be retained in a filter that must be periodically regenerated [4–6]. For warranting efficient removal of both contaminants, various combinations of these technologies have been proposed [7–9]. However, they all still suffer from serious drawbacks in view of their effective implementation, such as too high soot ignition temperature, lack of thermal and mechanical stability, high costs when noble metals are used.

Enhanced soot oxidation in the presence of NO_x has been widely demonstrated. In fact the "continuously regenerating-trap" (CRT) technology makes use of a Pt-supported catalysts upstream the particulate filter, allowing partial conversion of NO to NO_2, which is highly reactive towards the soot retained in the filter [10], therefore enhancing its oxidation. Therefore, it would be most desirable to attain at the same time and in one single device selective simultaneous reduction of NO_x to N_2 and complete soot removal. However, when using noble metal-based catalytic systems, like in CRT technology, only partial reduction of NO_2 to NO is achieved, with only small amounts of NO_x converted to N_2 [10]. On the other hand, other research groups reported successful NO_x conversion to N_2 [11–16],

* Corresponding author at: Department of Mechanical and Process Engineering, ETH Zürich, Sonneggstr. 3, 8092 Zürich, Switzerland. Tel.: +41 44 632 87 26.
E-mail addresses: megalvez@ethz.ch, megalvez@icb.csic.es (M.E. Gálvez).
[1] Present address: Department of Mechanical and Process Engineering, ETH Zürich,Sonneggstr. 3, 8092 Zürich, Switzerland.

0926-3373/$ – see front matter © 2014 Elsevier B.V. All rights reserved.
http://dx.doi.org/10.1016/j.apcatb.2014.01.041

in the presence of non-noble metal compounds, i.e. such as Cu, Co and V oxides together with K-species as surface promoter [17–19]. Among other transition metal (TM) compounds iron oxides has been successfully used as active phase in several similar reduction-oxidation catalysts [20–22]. Its low price and innocuous chemical properties make of it an interesting option for the preparation of such catalytic systems.

It is well documented nowadays that the presence of an alkali promoter, such as potassium, can substantially enhance the soot oxidation activity of TMO based catalysts [23–30]. Generally, all these works agree that one of the main roles of the alkali promoter is to improve the contact between the soot particles and the catalytic active sites. This is due to the high mobility of K, especially when it is not tightly bound to the support or to the transition metal oxide lattice [29]. However, some studies already point to a more complex participation of the various potassium species in the reaction mechanism. In this sense, Legutko et al. [23,24] prepared potassium iron and manganese spinels and studied the role of the alkali in the soot oxidation, considering also the presence of NO in the reactant gas [25]. They attributed the enhancement in soot oxidation activity, observed mostly when K was effectively introduced into the Fe or Mn spinel structure, to the generation low work function phases (potassium ferrites and manganites) and formation of surface reactive oxygen species which initialized soot combustion process. In a similar way, Ura et al. [26] identified two main mechanisms in terms of potassium promotion: the enhancement of the oxygen surface mobility and the formation of oxygen vacancies in the oxygen sublattice of the perovskite $SrTiO_3$ structure, depending on the localization of potassium. Jiménez et al. [30] claimed that potassium enhanced the reactivity of superficial oxygen and that, moreover, it was able to weaken the Mg–O bonds in the support, thus facilitating the formation and migration of oxygen species on the surface. Aneggi and co-workers [27] stated however that the effect of the alkali metal was to favor the chemisorption of molecular oxygen leading to the formation of carbon–oxygen surface complexes that eventually reacted with soot. In this sense, the alkali was acting as an oxygen carrier, transferring the oxygen from the gas phase to the surface carbon. Still, the mechanistic role of potassium remains unclear and it seems to depend on the catalytic system studied an even on the details of the chosen preparation procedure. Furthermore, due to a high vapor pressure of alkalis there is an important issue regarding catalyst stability when using them as soot oxidation promoters. As pointed out by An and co-workers [29], the K-containing catalyst is degraded upon time, due to the sublimation of potassium during the exothermic soot combustion process. Clearly, the K-loss rate, and therefore the catalyst stability, will depend on the type of K-species present in the catalyst, thus on their interaction with the support and other components, i.e. TMO.

The aim of the present work is to identify and characterize in detail the diverse K-species present in the cordierite-monolith supported Fe–K/Al_2O_3 catalysts. Therefore, transformation of surface potassium species during catalyst calcination and soot oxidation with simultaneous NO_x reduction process was studied. Both powder and monolithic catalysts were considered (the former mostly in terms of physic-chemical characterization, the later used for the activity tests). The role of different surface potassium states in soot oxidation mechanism was addressed.

2. Experimental

2.1. Catalysts preparation

Alumina-based suspensions were prepared by sol–gel synthesis, containing either both iron as catalytically active compound and potassium as promoter ($K/Fe/Al_2O_3$), or only potassium (K/Al_2O_3) as reference material. Disperal 20 (Sasol GmbH), a highly dispersible boehmite, was used as the alumina precursor. Concentrated nitric acid (65 wt%, Panreac) was added as peptizing agent. Iron and potassium were introduced from respective nitrates, $Fe(NO_3)_3{\cdot}9H_2O$ (99% pure, Panreac) and KNO_3 (99% pure, Panreac), in amounts corresponding to 5 wt% Fe and/or 10 wt% K. Suspensions were stirred for 24 h. After this time, their pH and viscosity were determined using a Crison GLP 21+ pHmeter and a Brookfield DV-E viscosimeter, respectively, and repeated after 4 days of ageing time, in order to verify gel stabilization.

Table 1
Catalysts labeling and description.

Labeling	Catalyst form	Active components	Calcination temperature (°C)
FeK450	Powder	Fe, K	450
FeK450_M	Monolith	Fe, K	450
FeK650	Powder	Fe, K	650
FeK650_M	Monolith	Fe, K	650
K450	Powder	K	450
K450_M	Monolith	K	450
K650	Powder	K	650
K650_M	Monolith	K	650

For the preparation of the powder catalysts, an aliquot of each suspension was dried for 24 h at 60 °C, and subsequently calcined in an oven, either at 450 °C or at 650 °C, during 4 h. Finally, powder catalyst were ground and sieved to an average particle size of 100 μm.

The structured catalysts were prepared by means of the washcoating of cordierite monoliths ($2MgO{\cdot}2Al_2O_3{\cdot}5SiO_2$, Corning, 400 cells per square inch, cpsi), cut into cylindrical units of 1 cm diameter per 3 cm length. To warranty an homogeneous distribution inside the monolith channels, the suspensions were pumped through the cordierite structure with the aid of a peristaltic pump. After 30 min circulation time, the coated monoliths were dried in a rotating oven at 60 °C during 24 h, and subsequently calcined, either at 450 °C or at 650 °C, during 4 h. Weighting before and after the washcoating procedure evidenced an average catalyst loading on the cordierite surface of 100 mg/g. Table 1 presents a list of the catalysts prepared, their labeling and description.

2.2. Catalysts characterization

The prepared catalysts were physically and chemically characterized: X-ray diffraction (XRD, Rigaku MiniFlex powder diffractometer with Cu *K*α radiation at 10 mA and 10 kV, 2θ step scans of 0.02° and a counting time of 1 s per step), scanning electron microscopy (SEM-EDS, Hitachi S-3400 N coupled with EDS analysis, Röntec XFlash), Raman spectroscopy (Horiba Jobin Yvon HR800 UV, under green laser conditions) IR spectroscopy (Vertex 70, Bruker, transmission, MIR, KBr pellets), X-ray photoelectron spectroscopy (XPS, ESCA+, Omicron), temperature-programmed oxidation (TGA, SETARAM Setsys Evolution, 50 mL/min air, 25–900 °C, 10 °C/min), temperature-programmed reduction in H_2 (0.1 g catalyst, 50 mL/min 10% H_2–Ar, 25–950 °C, 5 °C/min, TCD detector), and N_2 adsorption at −196 °C (Micromeritics ASAP 2020), applying BET method for the calculation of sample's surface area, BJH and *t*-plot methods for the calculation of meso and micropore volume, respectively.

Catalyst elemental composition was analyzed by means of ICP–OES (Service central d'analyse, CNRS, Villeurbanne). Relative bulk amounts of aluminum, iron and potassium were determined with the use of Energy-Dispersive XRF spectrometer (Thermo Scientific, ARL QUANT'X). Powder samples were in form of pellets of 13 mm in diameter with a mass of 150 mg. X-rays in the range of

4–50 kV (1 kV step) were generated with use of Rh anode, the beam size was 1 mm and the window was made of beryllium. Detector used was 3.5 mm Si(Li) drifted crystal with Peltier cooling (~185 K). For quantitative analysis, UniQuant software was used with a series of metallic standards.

The stability of potassium was investigated by the SR–TAD method, analogously to the approach applied in Ref. [31]. The experiments were carried out in a vacuum apparatus with a background pressure of 10^{-7} mbar. The pelletized powder samples, after XRF analysis, were transferred to the vacuum chamber and heated from room temperature to 600 °C and then cooled down by steps of 20 °C. Earlier desorption studies of potassium from styrene catalysts [32–34] and related ferrite phases [31,35] demonstrated that the K loss occurs mainly in the form of atoms. The desorption flux of potassium atoms, j_K, was determined by means of a surface ionization detector [36]. Because the investigated samples are also electron emitters, for quenching the thermal emission of electrons during the measurements, the samples were biased with a positive potential (+5 V for K). In all of the measurements, the resultant positive current was measured directly with a digital electrometer (Keithley 6512) and averaged over 10 independent data points for each temperature.

NO_x adsorption–desorption experiments were performed in a lab-scale installation prepared for working with one coated monolith, consisting of a tubular quartz reactor heated up by an electric oven and equipped with a battery of mass-flow controllers. The same experimental unit was employed for the activity tests described below. In the adsorption–desorption tests, 50 mL/min of gas mixture containing aprox. 500 ppmv NO, 5% O_2 in Ar were first flown through the monolithic catalyst, keeping temperature constant at 350 °C for 30 min. Let us remark here that 350 °C has been previously found to be the optimal temperature for nitrate formation upon NO_x adsorption on alkali compounds [3], this being the reason for our choice. After this adsorption step, gas flow was changed to 50 mL/min Ar, and temperature was increased from 350 to 650 °C, at 5 °C/min heating rate. Concentrations of CO, CO_2, NO, NO_2, N_2 and N_2O were continuously determined by mass spectrometry (MS Omnistar Balzers 442) and gas chromatography (Varian Micro GC CP 4900).

2.3. Activity tests

Prior to activity tests, soot filtration was simulated by means of loading a carbon black (Elftex 430, Cabot, S_{BET}: 80 m^2/g, primary particle mean size: 27 nm) to the surface of the structured monolithic catalysts. This carbon black was selected due to its identical behavior upon thermogravimetric oxidation in air, vis-à-vis laboratory-produced diesel soot. Still, the use of a carbon black can be considered as a conservative experimental approach, since the presence of soluble organic fraction (SOF) in real soot contributes to increased reactivity [37]. Each catalyst was introduced for 1 min into a continuously stirred dispersion of 0.2 g of carbon black in 100 mL *n*-pentane, then dried at 65 °C during 1 h. The amount of carbon black loaded corresponded approximately to 20 wt% load, with respect to the mass of catalytic material deposited on the surface of the monolith. As a result of this procedure loose contact between soot and catalyst is obtained, which is more representative of the real contact between the soot and the catalyst at the exit exhaust of an engine [38–40]. Electron microscopy (FE–SEM) characterization of the carbon-black loaded monolithic catalysts can be found in Ref. [19].

The activity of the prepared catalysts in the simultaneous removal of soot and NO_x was assayed in the previously described lab-scale installation. A reactant gas containing 500 ppmv NO and 5% O_2 in Ar was flown at 50 mL/min through a catalyst (1 cm diameter × approx. 3 cm length). Experiments were performed at temperatures between 250 and 650 °C, heating rate of 5 °C/min. Concentrations of the different compounds were analyzed by means of mass spectrometry and gas chromatography. Note that comparison of CO_2 concentration measured by gas chromatography to the corresponding *m/z* 44 signal determined in the mass spectrometer made it possible for us to practically rule out any possibility of N_2O formation.

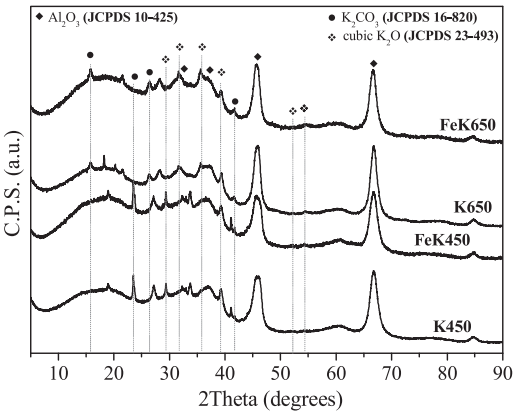

Fig. 1. Powder XRD pattern for FeK and K catalyst.

NO_x conversion, X_{NO} and X_{NO_x}, were calculated from the molar concentrations: $X_{NO} = m_{NO}/m^i_{NO}$ and $X_{NO_x} = (m_{NO} + m_{NO_2})/(m^i_{NO} + m^i_{NO_2})$, where *i* superscript denotes respective initial concentrations. Carbon black conversion, X_{CB}, was calculated using the initial amount of carbon black and the molar concentrations of CO and CO_2: $X_{CB} = (m_{CO_2} + m_{CO})/m^i_{CB}$.

3. Results and discussion

3.1. Physicochemical characterization

Physicochemical characterization yields important information about the structural and chemical features of the different catalyst prepared. XRD patterns for FeK and K powder catalysts, shown in Fig. 1, evidence the typical wide diffraction peaks of Al_2O_3. Within the region of 2θ between 15° and 45° several diffraction peaks can be observed, which can be assigned to either K_2CO_3 or K_2O. Calcination at 650 °C has an influence on the crystallinity and nature of K species present. In fact, peaks at 16° appear upon calcination at 650 °C, pointing to more pronounced presence of carbonates. Such carbonation of K-species may occur after calcination, during cooling process, as a consequence of the exposure of the catalysts to ambient air conditions. The reaction of CO_2 in air with K_2O to form K_2CO_3 is in fact thermodynamically favorable under such ambient conditions. The diffraction maxima due to iron containing phases are not clearly distinguished probably due to too small concentration and high dispersion on the support. SEM observation of the catalysts evidenced also the formation of potassium carbonate in the shape of characteristic needles of K_2CO_3 crystals, in the catalysts calcined at 650 °C (Fig. 2).

Textural parameters derived from N_2 adsorption isotherms are presented in Table 2. Surface area and pore volume values evidence higher pore blockage extent of the initial pore structure of the alumina in the case of the FeK catalysts, in comparison to K ones, and independently of the calcination temperature. Both powder catalysts, as well as the catalytic layer deposited on the surface of the cordierite monoliths in the structured catalysts, can be considered as mostly mesoporous, with average pore sizes around 14–17 nm.

Raman spectra acquired for the powder catalysts are presented in Fig. 3. The intense Raman band at 1050 cm^{-1} can be assigned to the presence of KNO_3. The band at 715 cm^{-1}, clearly seen in

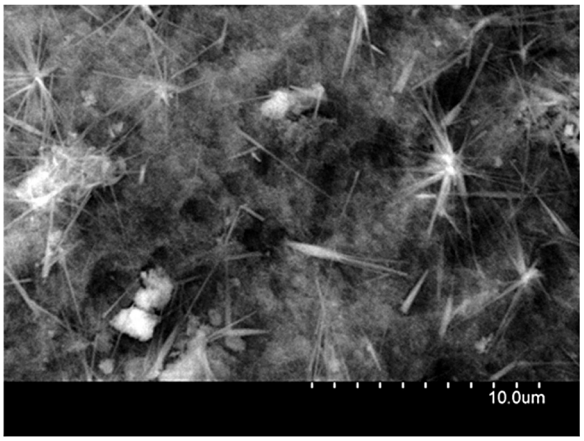

Fig. 2. SEM image for the FeK650 catalyst.

Table 2
Textural parameters derived from N_2 adsorption isotherms for the FeK and K powder (P) and monolithic (M) catalysts.

Catalyst	S_{BET} (m^2/g)	V_{pore} (cm^3/g)	V_{BJH} (cm^3/g)	Average pore size (nm)
FeK450	63.4	0.242	0.263	15
FeK450_M	6.6	0.023	0.024	14
FeK650	69.9	0.256	0.266	15
FeK650_M	8.7	0.031	0.031	14
K450	79.1	0.338	0.357	17
K450_M	8.8	0.032	0.033	15
K650	78.5	0.312	0.327	16
K650_M	7.1	0.027	0.027	15

the spectra for K450, still present in the spectra for K650 and less intense but yet visible in FeK650, is due as well to the presence of KNO_3. Seems thus that an important amount of nitrate species remain after catalyst calcination at 450 °C and are, on the other hand, more successfully decomposed when calcining at 650 °C. In fact, as a consequence of increasing calcination temperature from 450 to 650 °C a new band at about 1090 cm^{-1} appears in the spectra for FeK650 that was not observed for FeK450. This band can be ascribed to the presence of K_2CO_3. Though it can be seen as well in the spectra for K450, it becomes substantially more intense in that for K650, pointing to the transformation of potassium species upon calcination at higher temperatures. With respect to the iron oxide phase, Raman shows that in the catalysts calcined at 450 °C maghemite is the predominant phase, whereas at 650 °C this iron phase is transformed into hematite [41].

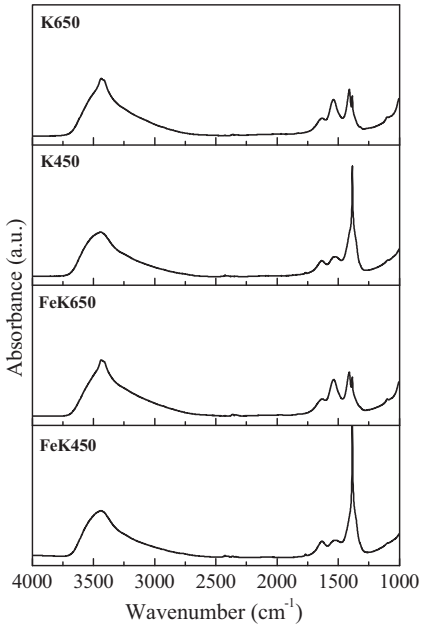

Fig. 4. Infrared spectra for the FeK and K catalysts.

Fig. 4 shows the IR spectra obtained for the powder catalysts calcined at 450 and 650 °C. Differing only slightly in the intensity

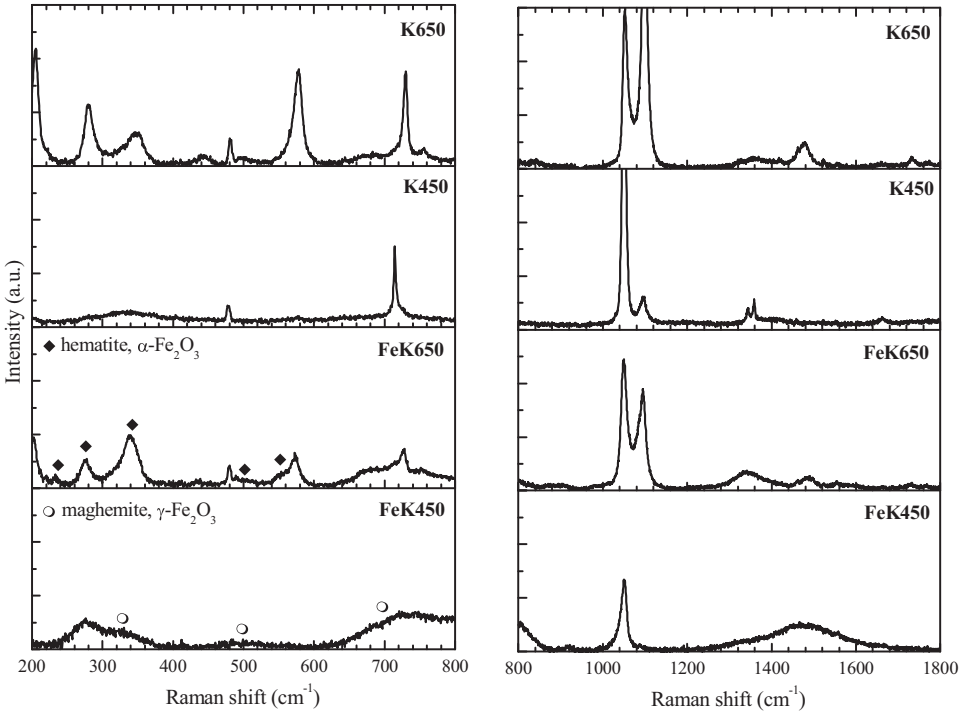

Fig. 3. Raman spectra for FeK and K catalysts.

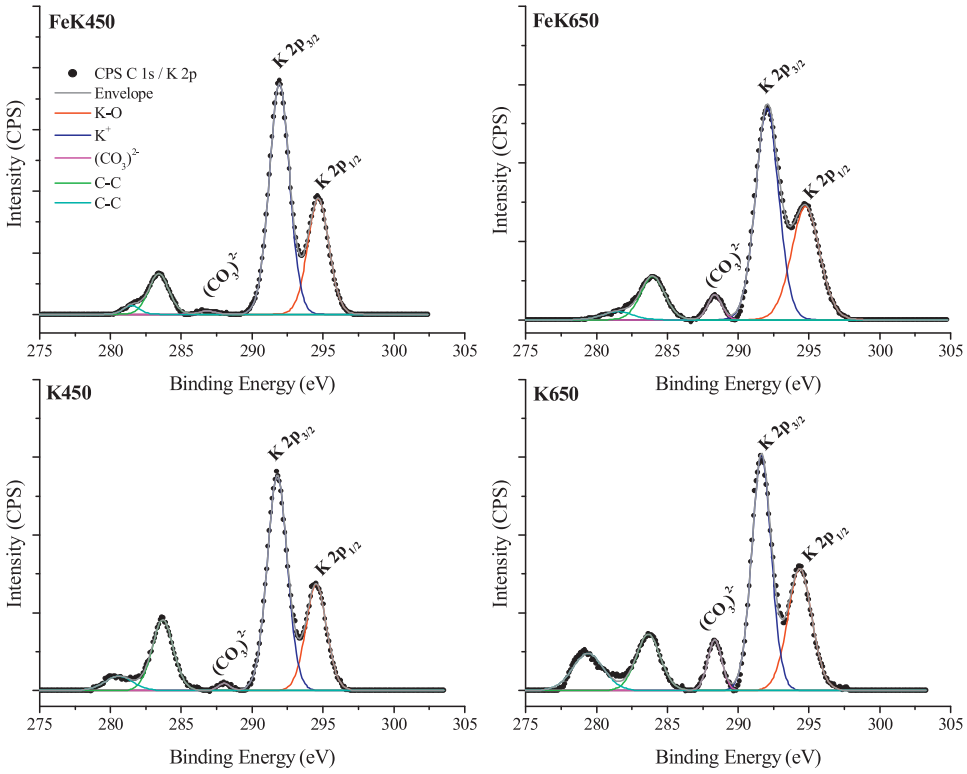

Fig. 5. XPS spectra C 1s/K 2p region for the FeK and K catalysts.

of IR bands, the spectra are almost identical for the catalysts prepared at the same calcination temperature. Bands in the range 3700–2600 cm^{-1} are due to the different–OH modes in the Al_2O_3 support [42–44]. The peak appearing about 3440 cm^{-1}, visible in the IR spectra of FeK650 and K650, can be assigned to the presence of potassium hydroaluminocarbonates [44].

With respect to potassium species, the sharp peak appearing in both K450 and FeK450 at about 1380 cm^{-1} evidences the presence of free nitrates, i.e. as a consequence of the presence of KNO_3 [45,46]. In agreement with Raman characterization, this fact points to the major presence of nitrate species in the catalysts calcined at the lowest temperature. The intensity of this peak is substantially reduced in the IR spectra corresponding to the catalysts calcined at 650 °C. On the other hand the intensity of the peak appearing at about 1540 cm^{-1} is substantially increased in the spectra for K650 and FeK650, which further confirms the conversion from KNO_3 to K_2CO_3. This band was assigned to C–O stretch of the chelating bidentate carbonate [47]. Similar bands have been reported in typical IR spectra of K_2CO_3/Al_2O_3 catalysts [44,48]. Thus, increased presence of carbonates is further confirmed, as a consequence of catalyst calcination at 650 °C. The wide nature of the IR bands in the range 1700–1200 cm^{-1}, makes it difficult, however, to distinguish among different carbonate species, i.e. weakly bonded $(CO_3)^{2-}$ ions or bidentate carbonates chemisorbed on K^+ or on alumina surface [44,49–51], pointing, more likely, to their coexistence. It is also possible, that some of the bands observed between 1700 and 1000 cm^{-1} arise also from $KAlCO_3(OH)_2$ or K-dawsonite, as its typical CO_3^{2-} bands are located at 1105 cm^{-1} (ν_1) and 1540 and 1450 cm^{-1} (ν_3). Also the bands arising from Al–OH tension oscillations lie within this range, at 1000 and 1072 cm^{-1} [52].

The presence of carbonates is further confirmed by XPS analysis. Fig. 5 shows the XPS spectra C 1s/K 2p region for the FeK and K powder catalysts calcined at 450 and 650 °C. In all the spectra, peaks appearing in the region 280–285 eV correspond to C 1s, due to impurities in the sample. Within the C 1s area, peaks in the range 287–290 eV have been generally assigned to the presence of carbonates [44]. The area of this peak notably increases in the case of the catalysts calcined at the highest temperature; see results in Table 2, therefore pointing to a higher abundance of carbonate species on the surface of FeK650 and K650 in comparison to those calcined at 450 °C. K 2p region is composed of a doublet with contributions at 292 eV and 294.7 eV which are, respectively, assigned to K $2p_{3/2}$ and K $2p_{1/2}$ potassium lines [53].

The Fe 2p XPS spectra of the powder FeK catalysts shows typical peaks due to contribution of both Fe^{2+} and Fe^{3+} [54–56]. In fact, peaks in the region 709–713 eV with a satellite at 725 eV are typical of Fe $2p_{3/2}$ and Fe $2p_{1/2}$ states in magnetite, Fe_3O_4. Deconvolution of Fe $2p_{3/2}$ peak can be performed considering a contribution of Fe^{2+} ions at 709–711 eV and another corresponding to Fe^{3+} ions at 711–713 eV [54]. Results are presented in Table 3. The presence of a certain amount of Fe^{2+} ions points to the co-existence of Fe_3O_4

Table 3
XPS analysis of C 1s/K 2p and Fe 2p regions for the FeK and K catalysts.

Catalyst	C 1s/K 2p			Fe 2p		
	Area $(CO_3)^{2-}$	K $2p_{3/2}$ (%)	K $2p_{1/2}$ (%)	Fe^{2+} (%)	Fe^{3+} (%)	Fe^{3+}/Fe^{2+}
FeK450	31.5	65.6	34.4	19.0	81.0	4.3
FeK650	252.9	60.3	39.7	13.3	86.7	6.5
K450	129.3	66.3	33.7	–	–	
K650	377.1	60.8	39.2	–	–	

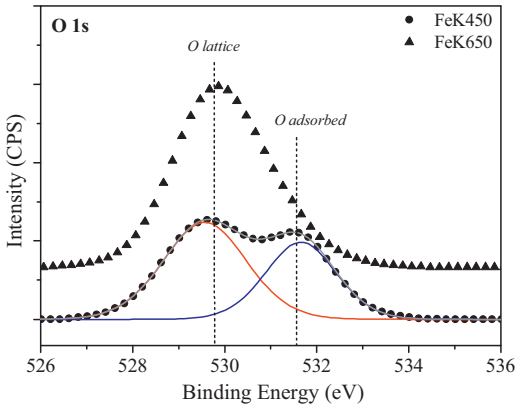

Fig. 6. XPS O 1s region for the FeK catalysts calcined at different temperatures.

Table 4
XPS analysis of O 1s region for the FeK and K catalysts.

Catalyst	O 1s			
	BE O 1s (eV)	FWHM (eV)	O lattice (%)	O adsorbed (%)
FeK450	529.6	3.9	59.8	40.2
FeK650	529.9	2.4	71.4	28.6
K450	529.6	3.1	68.5	31.5
K650	530.1	2.1	87.4	12.3

and Fe_2O_3 phases. Moreover, Fe^{3+}/Fe^{2+} ratio is all the time higher than 2 – the expected value for magnetite – meaning that mostly Fe_2O_3 is present on the surface of the FeK catalysts, in agreement with the results of Raman characterization.

Changes in surface composition as a consequence of calcination temperature have also an impact on O 1s peak shape and position. XPS O1 s spectra are plotted in Fig. 6. O 1s region can be deconvoluted into two peaks, which correspond to two forms of oxygen having different environments, i.e. lattice oxygen contained in metal oxides and adsorbed oxygen species, i.e.–OH groups [57]. The results of this deconvolution, as well as O 1s position and width (FWHM), are presented in Table 4. It becomes clear from the plots in Fig. 6 that O 1s peak shifts to lower BE values and becomes thinner with increasing calcination temperature, both for FeK and for K catalysts (see as well the values in Table 4, i.e. with increasing calcination temperature content in O lattice increases in all cases).

Further information on the chemical composition of the catalyst can be obtained from the temperature programmed reduction (TPR) experiments. Fig. 7 shows the TPR profiles obtained for the FeK and K powder catalysts. K-catalysts show an H_2 consumption peak at 550 and 490 °C, for K450 and K650, respectively. Calcination

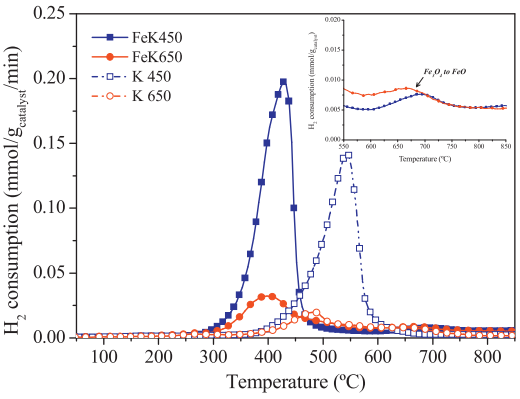

Fig. 7. Temperature programmed reduction (TPR) curves for the FeK and K catalysts.

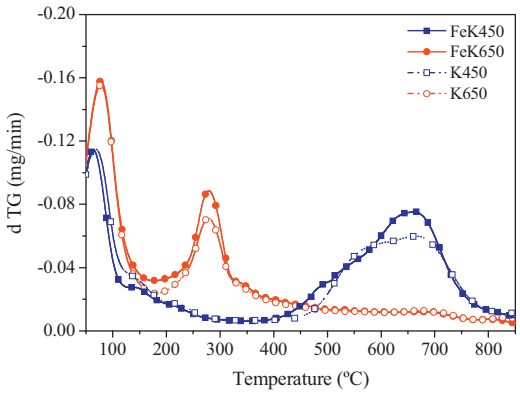

Fig. 8. Temperature programmed oxidation (TPO) curves for the FeK and K catalysts.

at higher temperatures results in a substantial decrease of H_2 consumption as well as in a shift to lower temperatures, pointing to higher reducibility of K-species. Marked H_2 consumption during TPR occurring at temperatures from 480 to 650 °C, such as that observed for K450, has been previously attributed to the presence of KNO_3 [58]. This can be due to the reduction of NO_3^- ions by H_2 to molecular nitrogen [59]. The presence of the same H_2 consumption peak for K650 may indicate the presence of some nitrate species on the surface of this catalyst remaining even after calcination at 650 °C.

The presence of Fe in the catalyst formulation results first of all in an increase in the reducibility of the K and/or Fe species, as pointed out by the shift to lower temperatures of the main peaks of H_2 consumption, i.e. at 430 °C for FeK450 and 390 °C for FeK650. According to literature [60,61] isolated Fe^{3+} ions undergo reduction at temperatures from 600 to 700 °C; whereas two-dimensional amorphous FeO_x clusters are reduced at about 500 °C, and three-dimensional Fe_2O_3 aggregates around 400 °C, closer to unsupported bulk Fe-oxides. Khan and Smirniotis [62] and Reddy et al. [54] reported a TPR peak at about 200–400 °C for the reduction of Fe_2O_3 to Fe_3O_4, which in our case may occur simultaneously to that corresponding to the reduction of K-species. Moreover, in agreement with XPS results, the presence of a magnetite phase is further confirmed by the appearance of a slight shoulder, represented in detail in the inset in Fig. 7, corresponding to the expected transformation of Fe_3O_4 to FeO at temperatures around 650 °C.

On the other hand, the behavior of the catalyst in the temperature programmed oxidation (TPO) experiments depended only on calcination temperature and not on catalyst formulation, i.e. presence of Fe. Curves for the powder catalysts are shown in Fig. 8. However, TPO profiles yield important information about the chemical state of the K-species in our catalysts. For both K450 and FeK450 the wide weight loss peak starting at a temperature around 400 °C and extending to temperatures as high as 800 °C can be assigned to the oxidation of the remaining nitrate species on both catalysts. After calcination at 650 °C, nitrates are no longer present, as pointed out by the disappearance of the wide peak observed in the catalysts calcined at 450 °C. A peak is observed now in the TPO profiles for K650 and FeK650, appearing at a temperature of 200 °C, centered at about 275 °C. This peak can be assigned to the decomposition of potassium carbonate species.

Normally, pure potassium carbonate decomposes at much higher temperatures, i.e. over 900 °C. However, decomposition of surface K-carbonate species has been reported to occur at much lower temperatures, due to their interaction with the support [43,45,47–49]. Therefore, decomposition is initiated by the interaction between K-carbonate species, K_2CO_3, and oxygen species, i.e. the hydroxyl groups on the Al_2O_3 surface, generating K^+ ionic

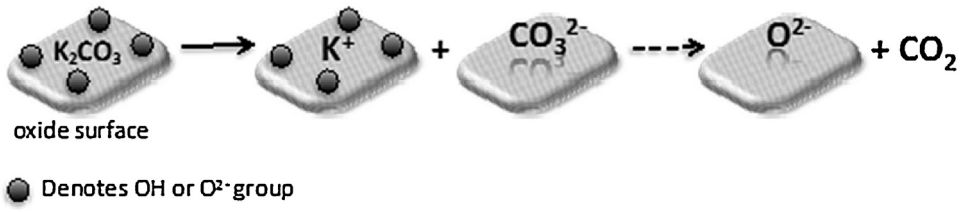

Fig. 9. Mechanism of formation of the active oxygen surface species via potassium carbonate decomposition upon interaction with the Al_2O_3 support.

species on the surface and adsorbed carbonates that, upon further heating, will yield O^{2-} species [63], as depicted in Fig. 9.

3.2. Temperature programmed desorption and NO_x adsorption–desorption experiments

Fig. 10a and b present the results obtained in the NO_x adsorption–desorption experiments performed for FeK450 and FeK650 monolithic catalysts. NO_x are adsorbed on the catalysts surface as can be deduced by the lower NO_x concentration measured during this first isothermal step. In the case of the catalyst calcined at the lower temperature, FeK450 in Fig. 10a, total amount of NO_x adsorbed represents 21.3% of the NO_x feed. The catalyst calcined at 650 °C, FeK 650 Fig. 10b, shows a higher ability to adsorb NO_x. Total NO_x adsorbed in this case amounts to 60.6% of the NO_x feed. During adsorption stage, CO_2 evolution is observed only during the first 15 min of experiment for FeK450, whereas for FeK650 CO_2 higher peak concentrations of CO_2 were measured and its evolution extending almost to the 30 min of adsorption stage. The observed CO_2 evolution is due to the thermal decomposition of carbonate species according to the mechanism depicted in Fig. 9.

Important differences are observed between desorption stages for FeK450 and FeK650. NO and NO_2 evolution starts already at about 375 °C for FeK450, almost right after switching to desorption conditions. In the case of FeK650, the evolution of nitrogen species begins at temperatures around 450 °C, at least 75 °C higher than for FeK650. Moreover, the amount of NO and NO_2 evolved is much higher in the case of FeK450. For FeK650, in fact, very small amounts of NO_2 were measured during the desorption stage. These results clearly point to the existence of different nitrogen species desorbing in each case. In the case of the catalyst calcined at 450 °C, FeK450, the desorption of NO and NO_2 can be mostly ascribed to the decomposition of nitrate species on its surface, still present after calcination. The 21.3% NO_x adsorbed during the first stage of course contributes as well to the observed desorption peak, but the rest, difference is 0.11 mmol NO_x, i.e. around 80% more NO_x desorbed than expected, can be assigned just to the presence and decomposition of such free nitrates.

On the other hand, nitrate species seem to be practically absent in the fresh catalyst calcined at 650 °C, whereas adsorbed N-species have increased stability and start desorbing at higher temperatures. This observation can be rationalized in terms of the formation of the additional basic oxygen species (O^{2-}) from carbonate decomposition, Fig. 9, which are stabilized by the adjacent potassium cations. On such O^{2-} sites adsorbed NO_2 was found to exhibit very high thermal stability, above 500 °C [64].

3.3. Potassium thermal desorption

The temperature changes of atomic K desorption fluxes (j_K) from investigated catalysts are presented in Fig. 11. All samples are stable below 400 °C with respect to potassium loss. Clear distinction can be made for the samples calcined at 450 and 650 °C, where lower calcination temperature leads to potassium desorption at temperatures lower of c.a. 100 °C. Comparison of the catalysts with and without iron addition reveals that for the samples calcined at 450 °C addition of iron leads to small enhancement of the desorption of

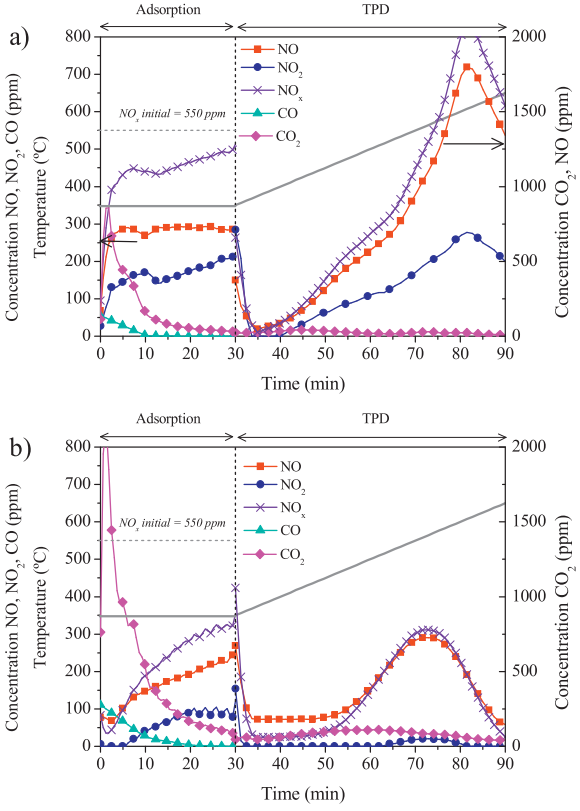

Fig. 10. NO_x adsorption–desorption NO, NO_2, CO and CO_2 concentration profiles for (a) FeK450 and (c) FeK650 catalysts.

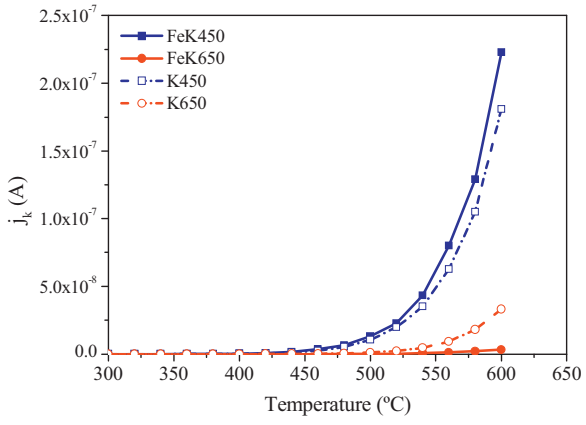

Fig. 11. Atomic K desorption flux (j_k) as a function of temperature for the investigated pelletized powder catalysts.

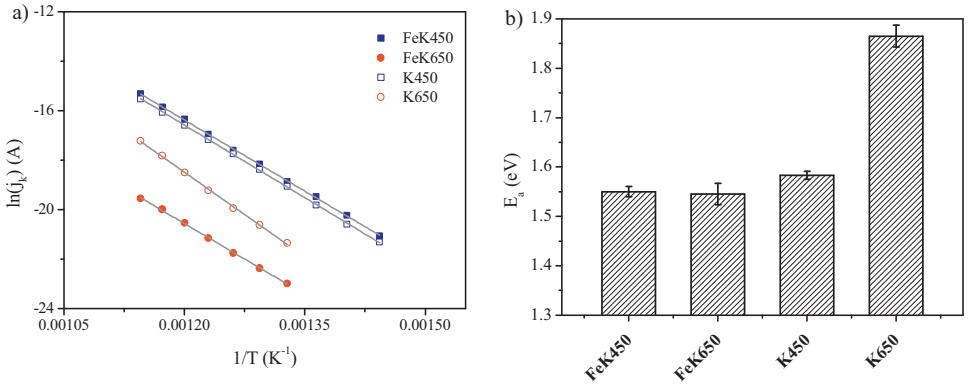

Fig. 12. (a) Arrhenius plots for the K-desorption; and (b) atomic potassium desorption activation energies for the different catalysts.

potassium while for those calcined at 650 °C iron addition results in dramatic decrease of K flux. Since during the thermal desorption experiment the K–surface bond is broken, the desorption parameters (flux intensity, activation energy, Arrhenius pre-exponential factor) describe not only the potassium surface stability but also contain the information about its surface state including dispersion [26].

Assuming first order desorption kinetics, the activation energy of desorption corresponding to each catalyst can be calculated from the linear part of the corresponding Arrhenius plots, which are shown in Fig. 12 a. Since the correlation coefficients for all of the investigated samples is higher than 0.999, the desorption activation energies can be determined with an error lower than 0.05 eV. Thus determined the desorption activation barriers are very similar for K450, FeK450 and FeK650 catalysts, regardless of their calcination temperature. The energy for K650 catalyst exhibit much higher value, see Fig. 12b. Differences in K desorption flux can be ascribed to different potassium species present and their surface coverage, as pointed out by the different pre-exponential factors obtained in the Arrhenius fitting. The obtained values of K desorption activation energies are typical for the iron and aluminum oxide surfaces with potassium in the segregated form [31–34,36,65], which is in line with the amount of the potassium added during the synthesis (10 wt%).

To clarify this point, we present in Table 5 the values obtained from the XPS analysis of the catalysts surface composition. Surface is in all cases notably enriched in K, whereas Fe content is far away from the nominal catalyst composition of 5 wt% This fact becomes more remarkable for the catalyst FeK450, showing the highest amount of K on its surface. XPS results are further corroborated by the results of SEM-EDX analysis of the catalysts where upon calcination at 650 °C the Fe/K ratio also substantially increases, as presented in Table 5. In this case the determined catalyst composition is closer to the nominal, though EDX still evaluates the first microns of the outer part of the catalysts surface. Once again, the catalyst presenting higher content of K on its surface is FeK450, whereas for FeK650 the percentages almost correspond to the nominal catalyst composition. ICP–OES analysis, accounting for the bulk content of the sample, yields Fe and K percentages close to the nominal ones. The same can be stated about the XRF analysis results. This fact confirms segregation of K species towards the outermost surface, occurring in most cases, but particularly for the catalyst FeK450. However, in spite of this migration of K to the outer surface of the catalysts, no important loss of K occurs upon calcinations and, moreover, no further loss can be observed as a consequence of increasing calcination temperature from 450 to 650 °C.

Thus, potassium loss upon calcination cannot be solely responsible for such a high decrease in the desorption signal. Possible reaction of iron and potassium species resulting in formation of ferrite phases is not supported by the structural analysis (Raman, XRD). The similar values of E_a for all catalysts, and the fact that no major effect of iron on the desorption signal is observed, suggest that, in all cases desorbing potassium is interacting mainly with Al_2O_3 support. As evidenced by SEM pictures (Fig. 2), during the calcination at 650 °C K_2CO_3 is segregated at the surface in the form of characteristic whiskers, leading to a decrease of the contact area between surface potassium and Fe/Al_2O_3 catalyst. This model is supported by the XPS results, where lower amounts of potassium was detected. Due to crystallization of K_2CO_3 into whisker form the higher amount of iron is exposed and thus available for direct XPS analysis, the surface Fe/K ratio increases substantially (Table 5). This transformation of surface potassium into crystalline potassium carbonate (Raman, XPS O1s) can moreover account for thermal stabilisation of K for the samples calcined at 650 °C.

3.4. Activity tests

Different potassium species generated upon calcination at different temperatures has a substantial influence on the catalytic activity. Figs. 13 and 14 show, respectively, the concentration profiles of NO, NO_2, N_2, CO and CO_2, as well as the NO_x and carbon black (CB) conversions, measured during the simultaneous deSoot and deNO_x activity tests performed in the presence of the different monolithic FeK and K monolithic catalysts.

Fig. 13a presents the concentration profiles registered as a function of temperature for the experiment performed using the

Table 5
Fe and K content (wt%) determined using different characterization techniques for the FeK and K catalysts.

Catalyst	XPS		SEM-EDX		ICP-OES		XRF	
	K (wt%)	Fe (wt%)	K (wt%)	Fe (wt%)	K (wt%)	Fe (wt%)	K (wt%)	Fe (wt%)
FeK450	55.1	0.58	29.8	6.8	8.9	4.5	12.0	6.1
FeK650	16.6	0.72	8.9	5.8	8.4	3.9	11.1	5.8
K450	13.8	–	17.7	–	8.8	–	11.6	–
K650	22.8	–	7.7	–	8.4	–	11.3	–

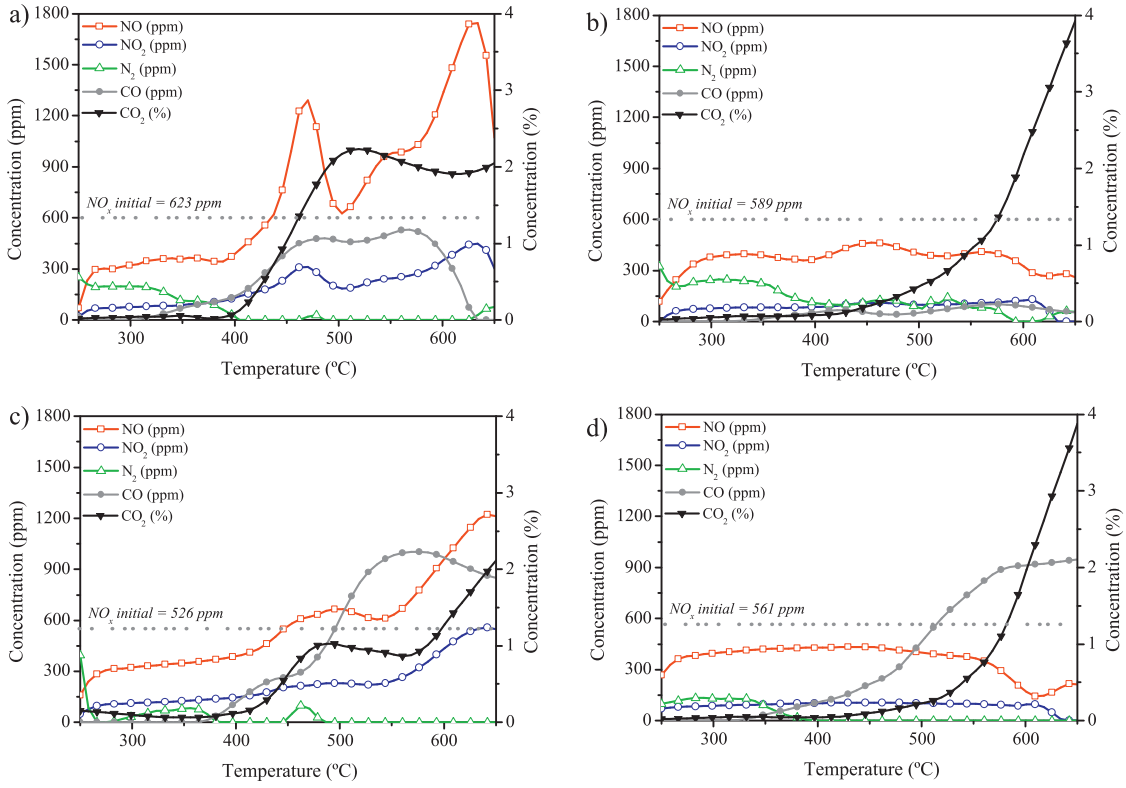

Fig. 13. Concentration profiles measured during the simultaneous removal activity tests, in the presence of (a) FeK450_M, (b) FeK650_M, (c) K450_M and (d) K650_M catalysts.

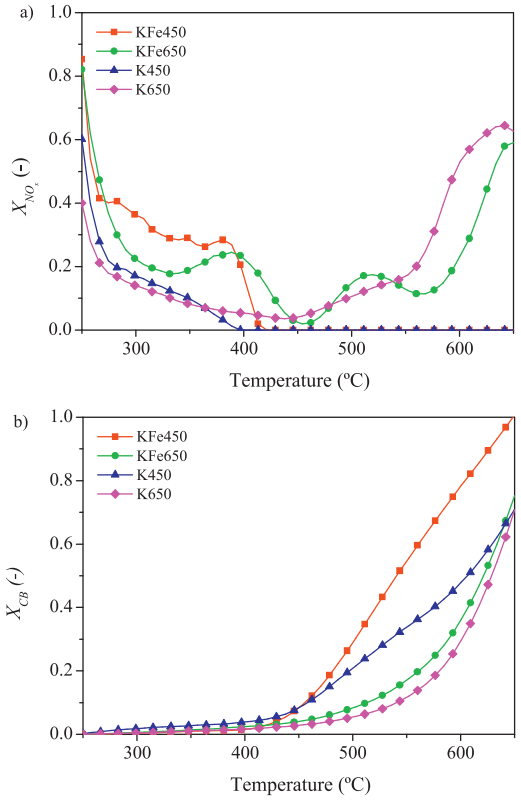

Fig. 14. (a) NO_x and (b) carbon black (CB) conversion as a function of reaction temperature measured during the activity tests in the presence of the different monolithic FeK and K catalysts.

FeK450_M catalyst. At temperatures from 250 to 400 °C NO_x adsorption takes place to some extent. This first stage of low NO_x concentration is followed by a progressive increase of NO and NO_2 concentration, due to the set-off of the decomposition of the thermally less stable free nitrate ions remaining on catalyst decomposition, as pointed out by its characterization and the results obtained in the adsorption–desorption tests. Corresponding to this NO and NO_2 evolution, soot oxidation starts taking place, accelerated by the enhanced presence of NO_2. Thus, a fast increase of CO_2 and CO concentrations can be observed within this temperature window, i.e. 400–500 °C. As temperature increases, NO and NO_2 concentrations start to decrease. The temperature at which minimal NO and NO_2 concentrations are attained corresponds to the maximal CO_2 evolution, pointing to maximal soot oxidation rate at that point. A slight increase in N_2 concentration was concurrently detected, pointing to some selective NO_x reduction taking place, together with simultaneous oxidation of the carbon black. However, due to a decreasing concentration of carbon black on the catalyst surface, and to the further decomposition or desorption of nitrogen species at higher temperatures, NO and NO_2 concentrations increase again from 550 °C and on. Carbon black oxidation continues, but at a much lower rate. Fig. 14a shows that in spite of the decrease observed in NO and NO_2 concentrations within the interval 450–550 °C, almost negligible NO_x conversion was observed for this FeK450_M catalyst. Note that NO_x conversion at low temperatures can be assigned mostly to adsorption and not of any kind of chemical reaction. On the other hand, Fig. 14b, shows that this FeK450_M catalyst was able to fully oxidize the carbon black deposited on its surface.

The concentration profiles determined during the experiment performed in the presence of the K450_M catalyst, Fig. 13c, follow a quite similar trend than the previously commented for the FeK450_M one. However, for K450_M, CO production is higher, and both NO_x adsorption capacity and carbon black oxidation activity

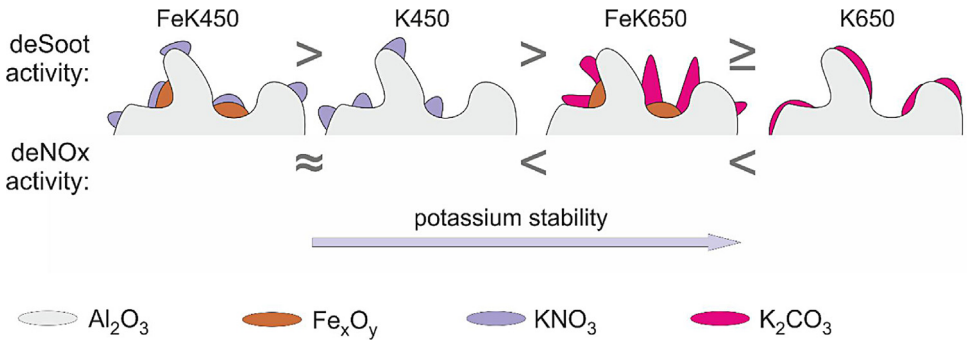

Fig. 15. Schematic representation of the K–Fe/Al_2O_3 catalyst morphology and distribution of the components.

are lower, as seen in Fig. 14a and b, pointing to a positive influence of the presence of Fe in the catalyst formulation, in terms of catalyst activity and selectivity.

Totally different concentration profiles were obtained for the catalyst calcined at the highest temperature. In the case of FeK650_M, Fig. 13b, NO_x adsorption is extended towards higher temperatures and no marked NO and NO_2 evolution can be observed. Carbon black oxidation sets-off at somehow higher temperatures as well, about 50 °C higher. However, the most remarkable difference is in the soot oxidation rate, which becomes maximal at much higher temperatures than for the catalyst calcined at 450 °C. Corresponding to this increase in the oxidation rate of the carbon material, a decrease in the concentration of both NO and NO_2 can be observed.

Taking into account all the facts evidenced by catalyst characterization and the adsorption desorption tests, it seems that the N-species adsorbed onto the basic O^{2-} surface groups generated upon decomposition of carbonate species, are thermally more stable and evolve from catalyst surface at somehow higher temperatures than those at which free nitrate species already decomposed to yield NO and NO_2. Moreover, NO_2 production is much lower in the case of the FeK650_M catalyst than for FeK450_M. This results in a slower oxidation of the carbon black, which therefore shifts the simultaneous removal reaction to higher temperatures. Nevertheless, NO_x are more efficiently reduced over the FeK650_M than for FeK450_M, see Fig. 14a, although maximal carbon black oxidation attained at the end of the experiment is much lower than for the FeK450_M catalyst, Fig. 14b.

Once again, when Fe is missing in the formulation of the catalyst, see Fig. 13d for K650_M catalyst, CO is produced to a higher extent, pointing to lower oxidation selectivity of this catalyst, and NO_x adsorption capacity is substantially hindered, what further confirms the importance of the presence of this metal.

Based on the physicochemical characterization described in Sections 3.1 and 3.3 the summarizing tentative schematic picture of the catalyst morphology and distribution of the components can be proposed, Fig. 15. It illustrates the effect of calcination temperature on the potassium promoter phase transformation from nitrates into carbonates (RS, FTIR, XPS) and their interaction with both iron and aluminum oxides. The picture takes into account the following experimental observations: iron phase locates mainly in the pores of the support phase (decrease of pore volumes derived from N_2 adsorption); the stability of potassium phase increases substantially upon calcination at 650 °C (SR-TAD, K desorption flux); on the Al_2O_3 support in the absence of iron phase the K desorption activation energy is the highest for all samples (SR-TAD), which implies the strongest K–surface interaction; the change of the total amount of potassium due to calcination at 650 °C is negligible (ICP–OES, XRF), however, in the presence of iron potassium surface concentration decreases (Fe/K surface ratio substantially increases) but in the absence of iron potassium surface concentration increases (XPS). Summing up, in the presence of iron the calcination at 650 °C leads predominantly to the segregation of K_2CO_3 while for the Al_2O_3 support alone the enhanced potassium dispersion is mainly observed.

4. Conclusions

We prepared and characterized Fe–K/Al_2O_3 and K/Al_2O_3 catalysts supported on cordierite monoliths, and evaluated the influence of the calcination temperature, i.e. 450 and 650 °C, on the catalysts features and on their activity in soot oxidation in the presence of NO_x.

Calcination temperature influences the type of K species present in the catalyst. Calcination at 450 °C was not enough to fully decompose the nitrate species used in the preparation of the catalyst. Thus in the catalysts calcined at this temperature, K is present mostly in KNO_3 form. On the other hand, calcination at 650 °C successfully transformed KNO_3 into K_2O, which upon exposure to ambient air becomes carbonated forming K_2CO_3 species.

Carbonate species formed upon calcination at 650 °C undergo decomposition in the presence of the oxygen surface groups of the alumina support. As a consequence of this decomposition surface K^+ species are formed, and new carbonate species that further decompose yielding basic O^{2-} groups that are stabilized by the presence of nearby K^+ cations. NO_x species adsorb strongly on this O^{2-} sites. Such N-species have enhanced thermal stability and desorb at temperatures around 540 °C, 75 °C higher than those corresponding the set-off for the decomposition of free KNO_3 species.

Potassium thermal desorption analyses evidenced much lower K atom flux upon heating for the catalysts calcined at 650 °C. Carbonate formation, segregation resulting in lower concentration of K on the surface, as well as the presence of a more crystalline phase are the reasons for the observed stabilization of K-species in these catalysts.

Activity in soot oxidation in the presence of NO_x was evidently influenced by the different potassium species generated upon calcination of the catalysts at different temperatures. Soot oxidation rate is always higher for the catalysts calcined at 450 °C, this being mostly a consequence of the remarkable NO_2 evolution occurring at temperatures around 400 °C. On the other hand, the increased stability of the N-species adsorbed on the basic O^{2-} functionalities created upon carbonate decomposition in the catalyst calcined at 650 °C, resulted in slower soot oxidation. However, the catalysts calcined at 650 °C evidenced higher ability towards the reduction of NO_x, occurring simultaneously with the soot oxidation process. The presence of iron oxide phases was found to increase the complete of soot oxidation to CO_2. The obtained results allowed for proposing an overall schematic model of the catalyst morphology

and relative distribution of the active components (K, Fe) over the Al_2O_3 support.

Acknowledgments

Polish part would like to acknowledge the Polish National Science Center for funding awarded by the decision number DEC-2011/01/B/ST4/00574. On the Polish part the research was partially carried out with the equipment purchased thanks to the financial support of the European Regional Development Fund in the framework of the Polish Innovation Economy Operational Program (contract no. POIG.02.01.00-12-023/08).

S. Ascaso thanks the European Social Fund and CSIC for her JAE doctoral grant. M.E. Gálvez is indebted to the Spanish Ministry of Economy and Competitiveness (Secretaría de Estado de I + D + I) for her Ramón y Cajal contract.

References

[1] Regulation EC N. 171/2013.
[2] A. Boyano, M.J. Lázaro, C. Cristiani, F.J. Maldonado-Hodar, P. Forzatti, R. Moliner, Chem. Eng. J. 149 (2009) 173–182.
[3] L. Castoldi, L. Lietti, P. Forzatti, S. Morandi, G. Ghiotti, F. Vindigni, J. Catal. 276 (2010) 335–350.
[4] S. Bensaid, D.L. Marchisio, D. Fino, Chem. Eng. Sci. 65 (2010) 357–363.
[5] P. Ciambelli, V. Palma, P. Russo, S. Vaccaro, Catal. Today 73 (2002) 363–370.
[6] B.R. Stanmore, J.F. Brilhac, P. Gilot, Carbon 39 (2001) 2247–2268.
[7] T.V. Johnson, Int. J. Engine Res. 10 (2009) 275–285.
[8] K. Nakatani, S. Hirota, S. Takeshima, K. Itoh, T. Tanaka, SAE Paper SP-1674, 2002-01-0957, 2002.
[9] C.-N. Millet, R. Chédotal, P. Da Costa, Appl. Catal., B 90 (2009) 339–346.
[10] B.J. Cooper, J.E. Thoss, SAE Paper 890404, 1989.
[11] K. Hizbullah, S. Kureti, W. Weisweiler, Catal. Today 93 (2004) 839–843.
[12] N. Nejar, M.J. Illán-Gómez, Appl. Catal., B 70 (2007) 261–268.
[13] D. Fino, P. Fino, G. Saracco, V. Specchia, Appl. Catal., B 43 (2003) 243–259.
[14] V.G. Milt, E.D. Banús, M.A. Ulla, E.E. Miró, Catal. Today 133–135 (2008) 435–440.
[15] H. Lin, Y. Li, W. Shangguan, Z. Huang, Combust. Flame 156 (2009) 2063–2070.
[16] W.F. Shangguan, Y. Teraoka, S. Kagawa, Appl. Catal., B 16 (1998) 149–154.
[17] M.E. Gálvez, S. Ascaso, I. Suelves, R. Moliner, R. Jiménez, X. García, A. Gordon, M.J. Lázaro, Catal. Today 176 (2011) 361–364.
[18] M.E. Gálvez, S. Ascaso, I. Tobías, R. Moliner, M.J. Lázaro, Catal. Today 191 (2012) 96–105.
[19] M.E. Gálvez, S. Ascaso, R. Moliner, M.J. Lázaro, Chem. Eng. Sci. 87 (2013) 75–90.
[20] M.L. Cubeiro, H. Morales, M.R. Goldwasser, M.J. Pérez-Zurita, F. González-Jiménez, C. Urbina de N., Appl. Catal., A 189 (1999) 87–97.
[21] B.C. Enger, R. Lodeng, A. Holmen, Appl. Catal., A 346 (2008) 1–27.
[22] C.W.B. Bezerra, L. Zhang, K. Lee, H. Liu, A.L.B. Marques, E.P. Marques, H. Wang, J. Zhang, Electrochim. Acta 53 (2008) 4937–4951.
[23] P. Legutko, T. Jakubek, W. Kaspera, P. Stelmachowski, Z. Sojka, A. Kotarba, Catal. Commun. 43 (2014) 34–37.
[24] P. Legutko, P. Stelmachowski, T. Trebala, A. Kotarba, Top. Catal. 56 (2013) 489–492.
[25] P. Legutko, W. Kaspera, T. Jakubek, P. Stelmachowski, A. Kotarba, Top. Catal. 56 (2013) 745–749.
[26] B. Ura, J. Trawczynski, A. Kotarba, W. Bieniasz, M.J. Illán-Gómez, A. Bueno-López, F.E. López-Suárez, Appl. Catal., B 101 (2011) 169–175.
[27] E. Aneggi, C. de Leitenburg, G. Dolcetti, A. Trovarelli, Catal. Today 136 (2008) 3–10.
[28] R. Matarrese, L. Castoldi, L. Lietti, P. Forzatti, Catal. Today 136 (2008) 11–17.
[29] H. An, P.J. McGinn, Appl. Catal., B 62 (2006) 46–56.
[30] R. Jiménez, X. García, C. Cellier, P. Ruiz, A.L. Gordon, Appl. Catal., A 297 (2006) 125–134.
[31] A. Kotarba, I. Kruk, Z. Sojka, J. Catal. 211 (2002) 265–272.
[32] L. Holmlid, P.G. Menon, Appl. Catal., A 212 (2001) 247–255.
[33] L. Holmlid, K. Engvall, C. Aman, P.G. Menon, Stud. Surf. Sci. Catal. 75 (1992) 795–807.
[34] K. Engvall, L. Holmlid, Appl. Surf. Sci. 55 (1992) 303–308.
[35] M. Muhler, R. Schlogl, G. Ertl, J. Catal. 138 (1992) 413–444.
[36] K. Engvall, L. Holmlid, A. Kotarba, J.B.C. Pettersson, P.G. Menon, P. Skaugset, Appl. Catal., A 134 (1996) 239–246.
[37] F. Bonnefoy, P. Gilot, B.R. Stanmore, G. Prado, Carbon 32 (1994) 1333–1340.
[38] J.P.A. Neeft, M. Makkee, J.A. Moulijn, Appl. Catal., B 8 (1996) 57–78.
[39] J.P.A. Neeft, M. Makkee, J.A. Moulijn, Appl. Catal., B 12 (1997) 21–31.
[40] E.D. Banús, V.G. Milt, E.E. Miró, M.A. Ulla, Appl. Catal., A 379 (2010) 95–104.
[41] D.L.A. de Faria, S. Venancio Silva, M.T. de Oliveira, J. Raman Spectrosc. 28 (1997) 873–878.
[42] S. Musić, D. Dragčević, S. Popović, Mater. Lett. 40 (1999) 269–274.
[43] M. Kantschewa, E.V. Albano, G. Etrtl, H. Knözinger, Appl. Catal. 8 (1983) 71–84.
[44] A. Iordan, M.I. Zaki, C.J. Kappenstein, Chem. Soc. Faraday Trans. 89 (1993) 2527–2536.
[45] Z.-Q. Zou, M. Meng, J.-J. He, Mater. Chem. Phys. 124 (2010) 987–993.
[46] M.A. Peralta, B.S. Sánchez, M.A. Ulla, C.A. Querini, Appl. Catal., A 393 (2011) 184–188.
[47] T.J. Toops, D.B. Smith, W.P. Partridge, Appl. Catal., B 58 (2005) 255–264.
[48] B. Hou, D. Parker, G.P. Kissling, J.A. Jones, D. Cherns, D.J. Fermín, J. Phys. Chem. C 117 (2013) 4089–4097.
[49] B.W. Krupay, Y. Amenomiya, J. Catal. 67 (1981) 362–370.
[50] F. Prinetto, M. Manyoli, S. Morandi, F. Frola, G. Ghiotti, L. Castoldi, L. Lietti, P. Forzatti, J. Phys. Chem. C 114 (2010) 1127–1138.
[51] T.J. Toops, D.B. Smith, W.P. Partridge, Catal. Today 114 (2006) 112–124.
[52] L. Fernández-Carrasco, F. Puertas, M.T. Blanco-Varela, T. Vázquez, J. Rius, Cem. Concr. Res. 35 (2005) 641–646.
[53] J.M. Moggia, V.G. Milt, M.A. Ulla, L.M. Cornaglia, Surf. Interface Anal. 35 (2003) 216–225.
[54] G.K. Reddy, P. Boolchand, P.G. Smirniotis, J. Catal. 282 (2011) 258–269.
[55] T.-C. Lin, G. Seshadri, J.A. Kelber, Appl. Surf. Sci. 119 (1997) 83–92.
[56] M.C. Biesinger, B.P. Payne, A.P. Grosvenor, L.W.M. Lau, A.R. Gerson, R.S.C. Smart, Appl. Surf. Sci. 257 (2011) 2717–2730.
[57] H. Wang, J. Liu, Z. Zhao, Y. Wei, C. Xu, Catal. Today 184 (2012) 288–300.
[58] S. Mosconi, I.D. Lick, A. Carrascull, M.I. Ponzi, E.N. Ponzi, Catal. Commun. 8 (2007) 1755–1758.
[59] L. Castoldi, L. Lietti, I. Nova, R. Matarrese, P. Forzatti, F. Vindigni, S. Morandi, F. Prinetto, G. Ghiotti, Chem. Eng. J. 161 (2010) 416–423.
[60] F. Arena, G. Gatti, G. Martra, S. Coluccia, L. Stievano, L. Spadaro, P. Famulari, A. Parmaliana, J. Catal. 231 (2005) 365.
[61] D. Prieto-Centurion, A.M. Boston, J.M. Notestein, J. Catal. 296 (2012) 77–85.
[62] A. Khan, P.G. Smirniotis, J. Mol. Catal. A 280 (2008) 43–51.
[63] T. Yamaguchi, Y. Wang, M. Komatsu, M. Ookawa, Catal. Surv. Jpn. 5 (2002) 81–89.
[64] C. Pazé, G. Gubitosa, S.O. Giacone, G. Spoto, F.X. Llabrés i Xamena, A. Zecchina, Top. Catal 30–31 (2004) 169–175.
[65] A. Kotarba, A. Barański, S. Hodorowicz, J. Sokołowski, A. Szytuła, L. Holmlid, Catal.Lett. 67 (2000) 129–134.